2011 American Control Conference
on O'Farrell Street, San Francisco, CA, USA
June 29 - July 01, 2011

Generalized Frequency Response of the Nonlinear Second Order System

Ashraf Omran and Brett Newman

***Abstract*—This paper develops generalized analytical first and second order transfer functions for the nonlinear second order system. A periodic input is also conducted to characterize the overall system response from the fundamental components. The proposed analytical solution provides more understanding of the influence of each linear and nonlinear component on the overall system behavior.**

I. Introduction

Many nonlinear dynamical systems can be analyzed with a simple mass-spring-damper system as a second order single degree of freedom (SDOF) model. Linearization provides a generalized solution given by a convolution integral in the case of time domain or by a transfer function in the case of s-domain. Classical linear metrics such as damping ratio and natural frequency or their equivalent transfer function's poles and zeros characterize the system's behavior. Unfortunately, linearization is restricted to small variations or first order derivatives. Even the use of the interpolation concepts to build a global linear parameter-varying model does not help in rendering some nonlinear phenomena such as limit cycle.

Looking for a method that one can use to extend the linear theory analysis to characterize the behavior of the nonlinear systems class, Volterra theory is the best choice primarily because of its underlying analytical framework or the so-called Volterra kernels. Volterra theory dates back to 1887 with the first encompassing publication appearing in 1927 and later in 1958 and it has been widely applied to model many dynamical systems [1]-[2]. For the second order SDOF system, more specifically, Refs.[3]-[9] developed higher order transfer functions or Volterra kernels of such a system but for specific test cases with no generalized conclusion. Previously in Refs. [10]-[11], the authors provided the desired generalized conclusion by developing analytical Volterra kernels to understand the influence of each linear and nonlinear system's parameters on the overall behavior of the nonlinear second order SDOF system. The main purpose of this paper is to construct the equivalent generalized frequency-domain analysis.

The rest of the paper is organized as follows: Section II briefly describes the mathematical foundation of Volterra theory and the algorithm to develop Volterra kernels or the high order transfer functions. A parametric study of the generic shapes of the first and second order transfer functions are set forth in Section III. In Section IV, a sinusoidal frequency response is developed. Section V gives a numerical example to show the merit of the developed analyses. Finally, in Section VI, the work is concluded.

Manuscript received Sep 21, 2010.

A. Omran is a research scientist and an adjunct assistant professor at Department of Mechanical and Aerospace Engineering, Old Dominion University., Norfolk, VA 23529, and an ASME Member. (corresponding author: phone:757-358-5892; fax: 757-683-3200; e-mail: aomra001@odu.edu).

B. Newman is a professor at Department of Mechanical and Aerospace Engineering, Old Dominion University., Norfolk, VA 23529, and an Associate Fellow AIAA. (e-mail: bnewman@odu.edu).

II. Volterra Theory

The nonlinear state $x \in R^n$ and output $y \in R^p$ model accounting for input $u \in R^m$ and time varying characteristics, for general dynamical systems, is

$$\begin{aligned} \dot{x}(t) &= f\left(t, x(t), u(t)\right) \\ y(t) &= g\left(t, x(t), u(t)\right) \end{aligned} \tag{1}$$

where vectors $f \in R^n$ and $g \in R^p$ denote the system nonlinearities. Volterra theory represents the input-output relation of a nonlinear system as an infinite sum of multi-dimensional convolution integrals [1].

$$\begin{aligned} y(t) &= \sum_{k=1}^{\infty} \int_0^{\infty} \int_0^{\infty} \cdots \int_0^{\infty} h_k(\tau_1, \tau_2, \ldots, \tau_k) \cdot \prod_{i=1}^{k} u(t-\tau_i) d\tau_i \\ Y(f) &= H_1(f) U(f) + \\ &\sum_{k=2}^{\infty} \int_0^{\infty} \int_0^{\infty} \cdots \int_0^{\infty} H_k\left(f_1, f_2, \ldots, f_{k-1}, f_k - \sum_{i=1}^{k-1} f_i\right) u\left(f_k - \sum_{i=1}^{k-1} f_i\right) \prod_{i=1}^{k-1} u(f_i) df_i \end{aligned} \tag{2}$$

In Eq. (2), $h_k(\tau_1, \tau_2, \ldots, \tau_k)$ is the k^{th} order Volterra kernel and $H_k(s_1, s_2, \ldots, s_k)$ is the k^{th} transfer function order where

$$H_k(s_1, \ldots, s_k) = \int \cdots \int h_k(\tau_1, \ldots, \tau_k) \prod_{i=1}^{k} e^{-s_i \tau_i} d\tau_i \tag{3}$$

In order to develop the kernels from the differential equation, variational expansion method is used. This method assumes the state vector derivative $\dot{x}$ is expandable as an infinite power series as

$$\dot{x} = f(x,u) = \sum_{i=0}^{\infty} \sum_{j=0}^{\infty} \widetilde{K}_{ij} x^{(i)} u^j, \; x^{(i)} = x \prod_{k=1}^{i-1} \otimes x \quad , \tag{4}$$

where $\otimes$ is Kronecker product. The matrix $\widetilde{K}_{ij}$ represents the derivatives of the vector function $f(x,u)$ with respect to $x^{(i)}$ and u^j at point (x_o,u_o). The input u is generalized to be $\alpha u(t)$, where α is any arbitrary constant. In this case, the response $x(t)$ can be expanded in terms of α as

$$x = \sum_{i=1}^{\infty} \alpha^i x_i \tag{5}$$

By substituting in Eq. (4) and rearranging according to the coefficients of equal α^i ($i = 1,2,\ldots$), a set of differential equations is generated as

$$\begin{aligned} \dot{x}_1 &= \widetilde{K}_{10} x_1 + \widetilde{K}_{01} u \\ \dot{x}_2 &= \widetilde{K}_{10} x_2 + \widetilde{K}_{20} x_1^{(2)} + \widetilde{K}_{11} x_1 u + \widetilde{K}_{02} u^2 \\ &\vdots \end{aligned} \tag{6}$$

Equation (6) represents the system as an infinite set of differential equations. The original nonlinearity of the system is broken into a sequence of pseudo-linear time

invariant (PLTI) systems, which are solvable. The input of each PLTI system is a nonlinear function of all previous system states and the input u. More details about this method are given in Ref. [11].

III. Analytical Transfer Functions

For the nonlinear second order SDOF system, assuming the quadratic and bilinear terms are enough to capture system nonlinearity in a certain neighborhood [14]-[16], the system is defined below.

$$\begin{aligned} \dot{x} &= v \\ \dot{v} &= -\omega_n^2 x - 2\varsigma\omega_n v + k_2 x^2 + c_k xv + c_2 v^2 + ku \qquad ku = F/m \end{aligned} \tag{6}$$

where ω_n is the undamped natural frequency, ζ the damping ratio, k_2 the secondary stiffness constant, c_2 the secondary damping constant, and c_k the bilinear stiffness-damping constant. In previous research [10], the author developed an analytical solution of such a system using Volterra model. The solution is given as

$$x \approx \int_0^t h_1(t-\tau)u(\tau)d\tau + \int_0^t\int_0^t h_2(t-\tau_1, t-\tau_2)u(\tau_1)u(\tau_2)d\tau_1 d\tau_2 \tag{11}$$

The expressions of $h_1(t)$ and $h_2(\tau_1,\tau_2)$ have been omitted from the current paper and they are given in Ref. [10]. Applying the Laplace transform given in Eq. (3), the equivalent transfer functions are

$$\begin{aligned} H_1(s_1) &= \frac{k}{s_1^2 + 2\zeta\omega_n s_1 + \omega_n^2} \\ H_2(s_1,s_2) &= H_2^{qp}(s_1,s_2) + H_2^{bpr}(s_1,s_2) + H_2^{qr}(s_1,s_2) \end{aligned} \tag{7}$$

where

$$H_2^{qp}(s_1,s_2) = \frac{k_2 k^2}{\left(s_1^2 + 2\zeta\omega_n s_1 + \omega_n^2\right)\left(s_2^2 + 2\zeta\omega_n s_2 + \omega_n^2\right)\left((s_1+s_2)^2 + 2\zeta\omega_n(s_1+s_2) + \omega_n^2\right)}$$

$$H_2^{bpr}(s_1,s_2) = \frac{0.5c_k k^2 (s_1+s_2)}{\left(s_1^2 + 2\zeta\omega_n s_1 + \omega_n^2\right)\left(s_2^2 + 2\zeta\omega_n s_2 + \omega_n^2\right)\left((s_1+s_2)^2 + 2\zeta\omega_n(s_1+s_2) + \omega_n^2\right)}$$

$$H_2^{qr}(s_1,s_2) = \frac{c_2 k^2 s_1 s_2}{\left(s_1^2 + 2\zeta\omega_n s_1 + \omega_n^2\right)\left(s_2^2 + 2\zeta\omega_n s_2 + \omega_n^2\right)\left((s_1+s_2)^2 + 2\zeta\omega_n(s_1+s_2) + \omega_n^2\right)}$$

The frequency response of the first transfer function is considered by replacing s by ωj as

$$\begin{aligned} H_1(j\omega) &= \frac{k}{\omega_n^2 - \omega^2 + 2\zeta\omega_n\omega j} \\ M_1(\omega) &= |H_1(j\omega)| = \frac{k}{\sqrt{\left(\omega_n^2 - \omega^2\right)^2 + (2\zeta\omega_n\omega)^2}} \\ \phi_1(\omega) &= \langle H_1(j\omega) = -\tan^{-1}\left(\frac{2\zeta\omega_n\omega}{\omega_n^2 - \omega^2}\right) \end{aligned} \tag{8}$$

The generic shape of the first kernel magnitude is shown in Figure 1. The frequency histories of M_1 start at value $M_{1o} = k/\omega_n^2$, while at ω tends to infinity, the value of M_1 tends to zero. There is a maximum peak defined by

$$M_{1\max} = \frac{k}{2\zeta\omega_n^2\sqrt{1-\zeta^2}} \quad \text{at} \quad \omega_c^l = \omega_n\sqrt{1-2\zeta^2} \tag{9}$$

This resonance peak exists only when $0 \le \zeta \le 0.707$. In the case of $\zeta > \sqrt{1/2} \approx 0.707$, this resonance diminishes.

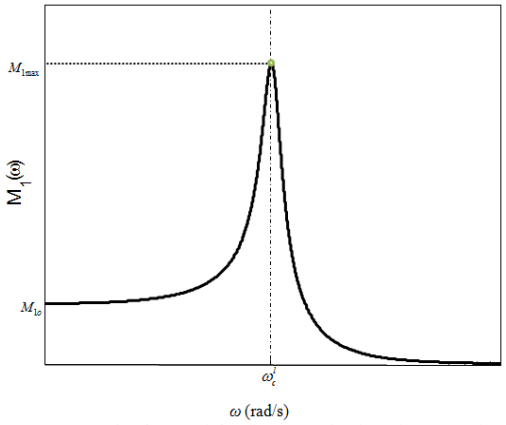

Figure 1 Generic shape of the first transfer function magnitude

The second transfer function has three components. The magnitudes and phases of these three components are

$$M_2^{qp}(\omega_1,\omega_2) = \left|H_2^{qp}(j\omega_1, j\omega_2)\right| = \frac{k_2 k^2}{\ell(\omega_1)\ell(\omega_2)\ell(\omega_1+\omega_2)} \tag{10}$$

$$M_2^{bpr}(\omega_1,\omega_2) = \left|H_2^{bpr}(j\omega_1, j\omega_2)\right| = \frac{0.5c_k k^2(\omega_1+\omega_1)}{\ell(\omega_1)\ell(\omega_2)\ell(\omega_1+\omega_2)}$$

$$M_2^{qr}(\omega_1,\omega_2) = \left|H_2^{qr}(j\omega_1, j\omega_2)\right| = \frac{c_2 k^2 \omega_1\omega_2}{\ell(\omega_1)\ell(\omega_2)\ell(\omega_1+\omega_2)}$$

$$\phi_2^{qp}(\omega_1,\omega_2) = \left\langle H_2^{qp}(j\omega_1, j\omega_2) = \vartheta(\omega_1) + \vartheta(\omega_2) + \vartheta(\omega_1+\omega_2)\right.$$

$$\phi_2^{bpr}(\omega_1,\omega_2) = \left\langle H_2^{bpr}(j\omega_1, j\omega_2) = 90^o + \vartheta(\omega_1) + \vartheta(\omega_2) + \vartheta(\omega_1+\omega_2)\right.$$

$$\phi_2^{qr}(\omega_1,\omega_2) = \left\langle H_2^{qr}(j\omega_1, j\omega_2) = -180^o + \vartheta(\omega_1) + \vartheta(\omega_2) + \vartheta(\omega_1+\omega_2)\right.$$

where

$$\ell(\omega) = \sqrt{\left(\omega_n^2 - \omega^2\right)^2 + (2\zeta\omega_n\omega)^2}$$

$$\vartheta(\omega) = -\tan^{-1}\left(\frac{2\zeta\omega_n\omega}{\omega_n^2 - \omega^2}\right)$$

The magnitude of the three components: quadratic position component $M_2^{qp}(\omega_1,\omega_2)$, bilinear position-rate component $M_2^{bpr}(\omega_1,\omega_2)$, and quadratic rate component $M_2^{qr}(\omega_1,\omega_2)$ are two-dimensional surfaces as functions of ω_1 and ω_2. Figures 2-8 show an example of each component at ω_n = 5 rad/s with different damping ratios ζ = {0.1, 0.4, 0.8}. There are some similarities among the shape of these surfaces. All the surfaces tend to zero when ω_1 and ω_2 tend to infinity. For a certain value of the damping ratio, there is a family of maximum points located on a line crossing the edges at $\{\omega_{e\max}^i, 0\}$ and $\{0, \omega_{e\max}^i\}$, while crossing the diagonal line at $\{\omega_{d1\max}^i, \omega_{d1\max}^i\}$, where i = {*qp*, *bpr*, *qr*}.

On the other hand, there are some dissimilarities among these surfaces. Unlike the bilinear position-rate magnitude $M_{20}^{bpr}(0,0) = 0$ and quadratic rate magnitude $M_{20}^{qr}(0,0) = 0$, the

quadratic position magnitude has a non-zero value $M_{20}^{bpr}(0,0)=k_2k^2/\omega_n^6$. In the case of the quadratic position magnitude surface $M_2^{qp}(\omega_1,\omega_2)$, there are two critical damping ratios $\zeta_{c1}^{qp}=0.21$ and $\zeta_{c2}^{qp}=0.707$. If $0<\zeta<\zeta_{c1}^{qp}$, the surface $M_2^{qp}(\omega_1,\omega_2)$ has a family of maximum points in addition to the two single maximum and minimum values located on the diagonal line (see Fig. 2). When the value of ζ exceeds $\zeta_{c1}^{qp}=0.21$, the single maximum and minimum points on the diagonal line diminish (see Fig. 3). In the case of $\zeta>\zeta_{c2}^{qp}=0.707$, the family of the maximum point disappears and the surface $M_2^{qp}(\omega_1,\omega_2)$ has one global maximum point at the origin whereby $\omega_1=\omega_2=0$ (see Fig.4).

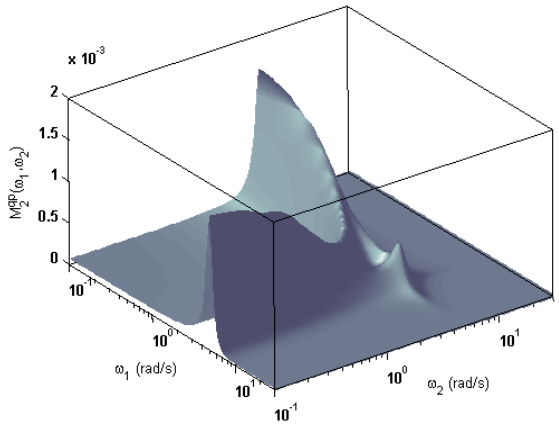

Figure 2 Quadratic position kernel magnitude at ω_n = 5 rad/s and ζ=0.1

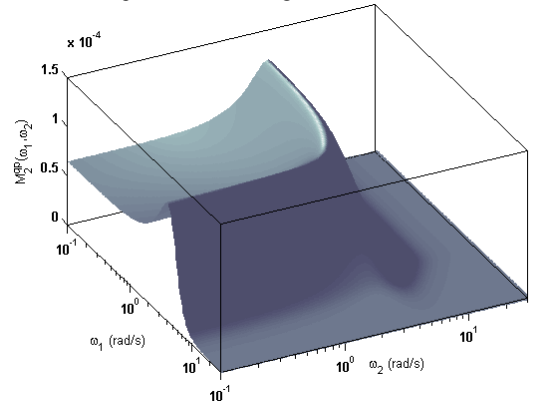

Figure 3 Quadratic position kernel magnitude at ω_n = 5 rad/s and ζ=0.4

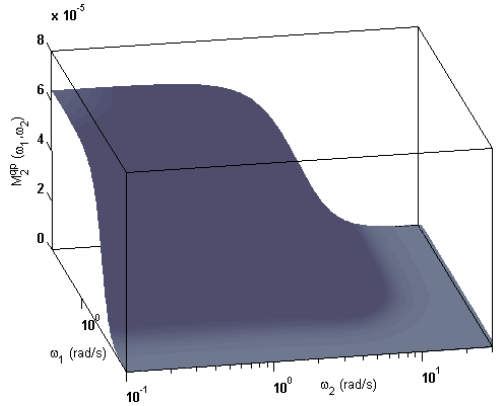

Figure 4 Quadratic position kernel magnitude at ω_n = 5 rad/s and ζ=0.8

Both the bilinear position-rate magnitude surface $M_2^{bpr}(\omega_1,\omega_2)$ and the quadratic rate magnitude surface $M_2^{qr}(\omega_1,\omega_2)$ have only one critical damping ratio $\zeta_{c1}^{bpr}=0.27$ and $\zeta_{c1}^{qr}=0.21$. When the damping ratio ζ exceeds $\zeta_{c1}^{bpr}=0.27$, the single maximum and minimum points on the diagonal line disappear on the surface $M_2^{bpr}(\omega_1,\omega_2)$ (see Fig. 6), while when $\zeta>\zeta_{c1}^{qr}$, the line presenting the family of maximum points and the single minimum point disappear on the surface $M_2^{qr}(\omega_1,\omega_2)$ (see Fig. 8).

Table 1 shows all the critical frequencies wherein these maximum and minimum values are located. Note there is an approximation using Taylor expansion applied to most of these critical frequencies in Table 1. For example, in the cases of $\omega_{e\max}^{bpr}$ and $\omega_{e\max}^{qr}$, the approximation was applied as

$$\omega_{e\max}^{bpr}=\omega_n\sqrt{\frac{1}{3}-\frac{2}{3}\zeta^2+\frac{2}{3}\sqrt{1-\zeta^2+\zeta^4}}\approx\omega_n\sqrt{1-\zeta^2} \qquad (11)$$

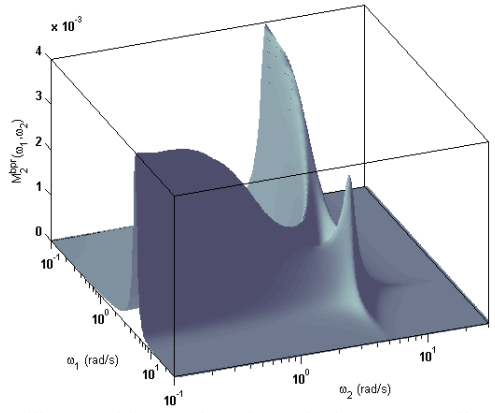

Figure 5 Bilinear position-rate kernel magnitude at ω_n = 5 rad/s and ζ=0.1

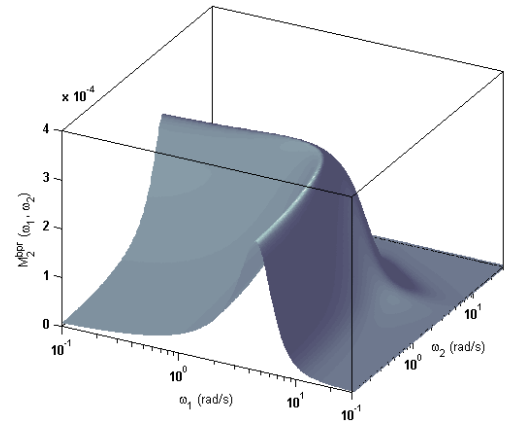

Figure 6 Bilinear position-rate kernel magnitude at ω_n = 5 rad/s and ζ=0.4

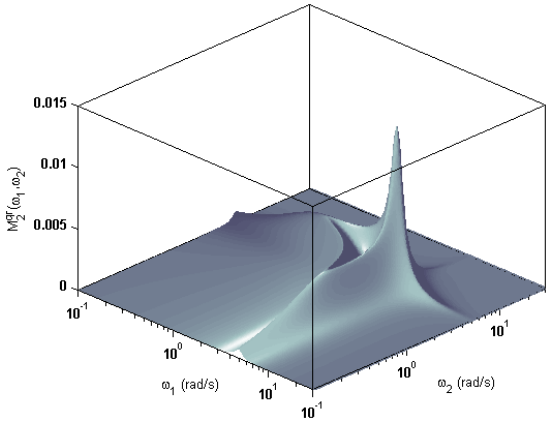

Figure 7 Quadratic rate kernel magnitude at ω_n = 5 rad/s and ζ=0.1

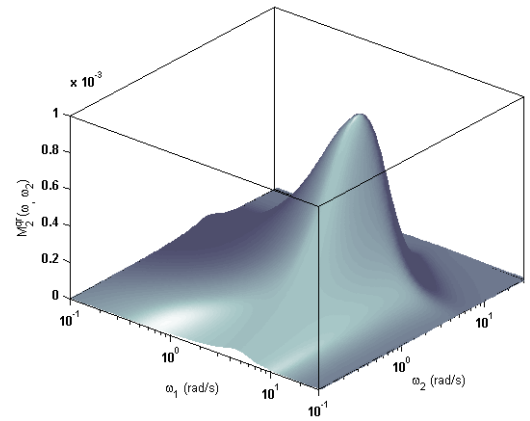

Figure 8 Quadratic rate kernel magnitude at ω_n = 5 rad/s and ζ =0.4

Table 1 Locations of optimal point on the nonlinear magnitude surfaces

Critical Frequency	Range
$\omega_{e\max}^{qp} = \omega_n\sqrt{1-2\zeta^2}$	$0<\zeta<0.7$
$\omega_{d1\max}^{qp} \approx \omega_n\sqrt{\frac{1}{4}+\frac{1}{6}\zeta^2}$	$0<\zeta<0.7$
$\omega_{d\min}^{qp} \approx \omega_n\sqrt{\frac{1}{2}+\zeta^2}$	$0<\zeta<0.21$
$\omega_{d2\max}^{qp} \approx \omega_n\sqrt{1-\frac{14}{3}\zeta^2}$	$0<\zeta<0.21$
$\omega_{e\max}^{qbpr} \approx \omega_n\sqrt{1-\zeta^2}$	$0<\zeta<1$
$\omega_{d1\max}^{bpr} \approx \omega_n\sqrt{\frac{1}{4}+\frac{2}{6}\zeta^2}$	$0<\zeta<1$
$\omega_{d\min}^{bpr} \approx \omega_n\sqrt{0.46-0.073\zeta^2}$	$0<\zeta<0.27$
$\omega_{d2\max}^{bpr} \approx \omega_n\sqrt{1-\frac{11}{3}\zeta^2}$	$0<\zeta<0.27$
$\omega_{e\max}^{qr} =\approx \omega_n\sqrt{1+\frac{14}{3}\zeta^2}$	$0<\zeta<0.21$
$\omega_{d1\max}^{qr} \approx \omega_n\sqrt{\frac{1}{4}+\frac{7}{6}\zeta^2}$	$0<\zeta<0.21$
$\omega_{d\min}^{qr} \approx \omega_n\sqrt{0.42-1.08\zeta^2}$	$0<\zeta<0.21$
$\omega_{d2\max}^{qr} \approx \omega_n\sqrt{1-\frac{8}{3}\zeta^2+\frac{80}{27}\zeta^4}$	$0<\zeta<1$

In order to simplify visualizing these surfaces, the diagonal line, whereby $\omega_1 = \omega_2 = \omega$, is considered to characterize the entire surface. At low damping ratio, when $0<\zeta<\zeta_{c1}^i$, where $i = \{qp, bpr, qr\}$, the diagonal line of all surfaces has two maximum values at $\omega_{d1\max}^i$ and $\omega_{d2\max}^i$ in addition to a minimum value at $\omega_{d\min}^i$ as shown in Fig. 9. If $\zeta>\zeta_{c1}^i$, the minimum value $\omega_{d\min}^i$ and one of the maximum point $\omega_{d1\max}^i$ or $\omega_{d2\max}^i$ disappear on all the surfaces, while the other maximum point stays as shown in Fig. 10. In the case of the quadratic position and bilinear position-rate components, the point $\omega_{d1\max}^i$ stays, while $\omega_{d2\max}^i$ disappears, while in the case of quadratic rate, $\omega_{d1\max}^i$ disappears and $\omega_{d2\max}^i$ stays for $\zeta>\zeta_{c1}^i$ (see Fig. 10). Figure 11 shows a special case of the quadratic position magnitude diagonal line at $\zeta>\zeta_{c2}^{qp}=0.707$, wherein all the maximum and minimum points diminish and the diagonal line starts at M_0^{qp} heading downward to settle at zero value when ω goes to infinity.

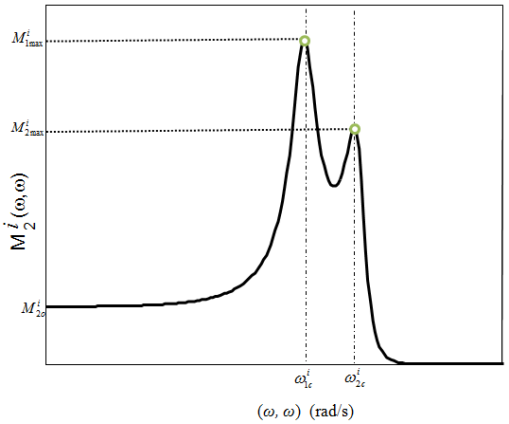

Figure 9 Magnitude diagonal of the component i = {qp, bpr, qr} for $\zeta < \zeta_{ci}$

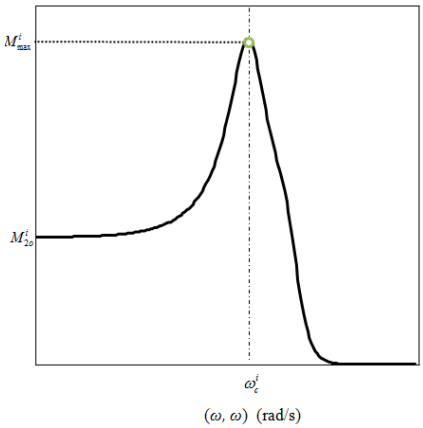

Figure 10 Magnitude diagonal of the component i = {qp, bpr, qr} for $\zeta > \zeta_{ci}$

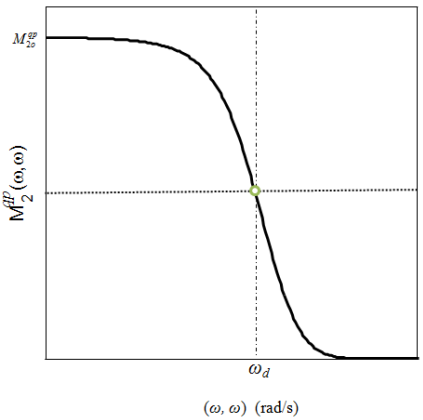

Figure 11 Magnitude diagonal of the component i = {qp, bpr, qr} for $\zeta > \zeta_{ci}$

There is no existence of any maximum or minimum peak on any of the phase surfaces $\phi_2^{qp}(\omega_1,\omega_2)$, $\phi_2^{bpr}(\omega_1,\omega_2)$, and $\phi_2^{qr}(\omega_1,\omega_2)$. All the surfaces have their equivalent maximum value at $\omega_1=\omega_2=0$ and they keep decreasing to achieve their equivalent minimum values at $\omega_1=\omega_2=\infty$. Figure 12 shows an example of the phase surface $\phi_2^{qp}(\omega_1,\omega_2)$ at ω_n =

5rad/s and ζ = 0.3. The generic shape of the diagonal line can describe the phase surface as shown in Fig. 13. All the diagonal lines start by their maximum value $\phi_2^{qp}(0,0)=0$, $\phi_2^{bpr}(0,0)=90^o$, $\phi_2^{qr}(0,0)=-180^o$ and they reach their minimum values $\phi_2^{qp}(\infty,\infty)=-360^o$, $\phi_2^{bpr}(\infty,\infty)=-270^o$, $\phi_2^{qr}(\infty,\infty)=-540^o$. When $\omega=\omega_n$, the value of the $\phi_2^i(\omega_n,\omega_n)=0.5\left(\phi_2^i(0,0)+\phi_2^i(\infty,\infty)\right)$, where i = {pq, bpr, qr}. The slope of $\mathrm{d}\,\phi_2^i(\omega_n,\omega_n)/\mathrm{d}\,\omega$ indicates the way that every diagonal line changes from its equivalent zero value to infinity value. The less damping ratio the system has, the more increase in the value of the slope $\mathrm{d}\,\phi_2^i(\omega_n,\omega_n)/\mathrm{d}\,\omega$ would be observed (see Fig. 13). The phase of the first transfer function is the same as in Fig. 13 starting with , $\phi_1(0,0)=0^o$ and then heading downward to settle at $\phi_1(\infty,\infty)=-180^o$.

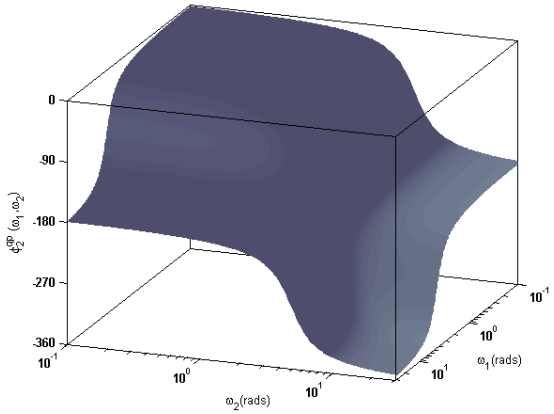

Figure 12 Quadratic position kernel magnitude at ω_n = 5 rad/s and ζ=0.3

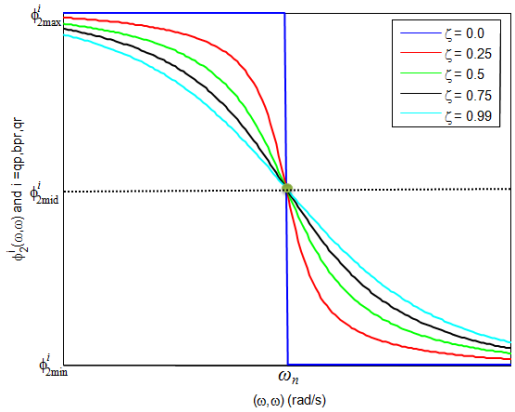

Figure 13 Phase diagonal of the component i = {qp, bpr, qr}

IV. Steady Sinusoidal Response

Following the same rationale of the linear theory, consider the sinusoidal response more specifically. If the input signal is a sinusoidal signal $u(t) = \sin(\omega t)$, the approximate nonlinear response is computed from the two terms Volterra series as

$$x = x_1 + x_2^{qp} + x_2^{bpr} + x_2^{qr} \tag{12}$$

The responses of the linear term x_1 and the nonlinear components x_2^{qp}, x_2^{bpr}, and x_2^{qr} have two parts: transient response and steady periodic response. In order to describe the overall response, describing the steady periodic responses is considered herein. Using the time convolution integral or the frequency response in Eq. (2) leads to

$$\begin{aligned} x_{1ss} &= A_l \sin(\omega t + \phi_l) \\ x^i_{2ss} &= K^i_{dc} + A^i_2 \sin\left(2\omega t + \phi^i_2\right), \quad i = \{qp, bpr, qr\} \end{aligned} \tag{13}$$

where

$$A_l = AM_1$$

$$A_2^{qp} = \frac{1}{2}A^2 M_2^{qp} \qquad K^i_{dc} = \frac{1}{2}A^2 M_l^2$$

$$A_2^{bpr} = \frac{1}{2}A^2 M_2^{bpr} \qquad K^i_{dc} = 0$$

$$A_2^{qr} = \frac{1}{2}A^2 M_2^{qr} \qquad K^i_{dc} = \frac{1}{2}A^2 M_l^2 \omega^2$$

The results in Eq. (13) show the relation between the magnitudes and the phases of the transfer functions and the individual response of each linear and nonlinear component in the systems. The linear term x_1 has a steady sinusoidal response with the same input frequency ω but with an amplitude ratio M_1 and phase shift ϕ_l. Figure 14 shows the relation between the input u and the steady linear response x_1 as an ellipse. The aspect ratio of the ellipse is M_1. Increasing the phase from zero to 180 deg rotates this ellipse counter clockwise from 45 deg to 315 deg as shown in Fig. 14.

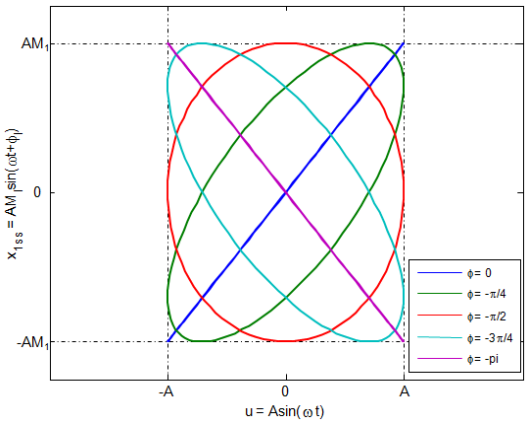

Figure 14 Linear periodic input-output relationship

Unlike the first term, all the components i = {qp, bpr, qr}of the second term x_2 are sine wave with double of the frequency of the input and a dc gain K^i_{dc} in addition to a phase shift ϕ^i_2 and an amplitude ratio $0.5M^i_2$. The relation between the input and these components' outputs is shown in Fig. 15 as a Lissajous shape.

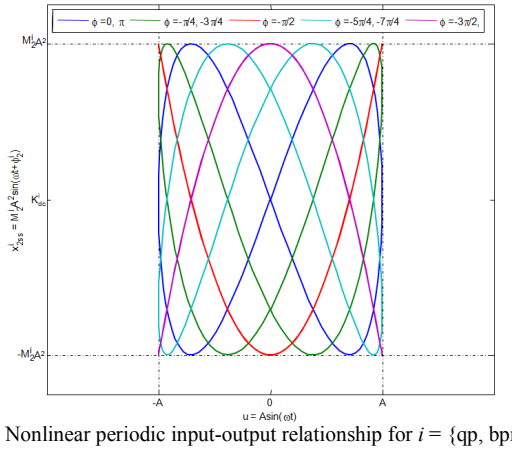

Figure 15 Nonlinear periodic input-output relationship for i = {qp, bpr, qr}

V. Numerical Example

Assume a force $F = 5\sin(\omega_d t)$ N excites a mass-spring-damper system; mathematically defined by

$$\ddot{x} = -0.6\dot{x} - 3x + 0.3x^2 + 0.25x\dot{x} - 0.3\dot{x}^2 + F \qquad (25)$$

The individual nonlinear components' responses are shown in Fig.16. Although all the nonlinear coefficients have almost the same value, from highest to lowest, the order of their oscillation's amplitudes are: quadratic rate, bilinear position-rate, and position quadratic component. All nonlinear components oscillate with the same frequency $2\omega_d$ = 3.4 rad/s, while the linear term oscillates by a frequency ω_d = 3.4 rad/s. Unlike the quadratic position and bilinear components, the quadratic rate component has a significant d.c gain with a value -0.093 m.

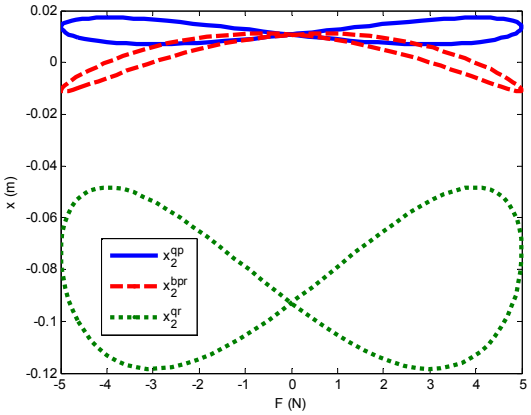

Figure 16 Nonlinear components periodic responses

Figure 17 shows the responses of nonlinear simulation, linear-based model, and Volterra-based model. It is clear how Volterra-based model more accurately duplicates the steady response of the system than the linear-based model. The relation between the input and output is a pure ellipse. Adding the nonlinear components leads to an imperfection of this elliptical shape. This imperfection is observed when the output signal is not a single tone frequency signal. In the linear case, the center of the ellipse is the origin, while the center of the resultant imperfect ellipse of the Volterra model is non-zero. This non-zero origin is observed as a nonsymmetrical oscillation due to the d.c gain generated by the quadratic rate nonlinearity.

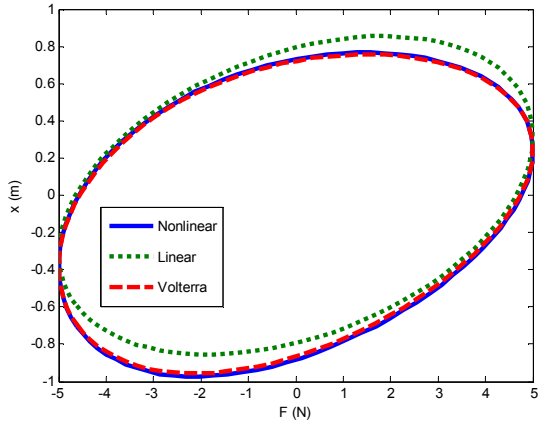

Figure 17 Overall periodic response

VI. Conclusion

This work offers a procedure to develop closed-form expressions for the second order system's kernels, which in turn leads to expressions for the sinusoidal input time response. The spring-mass-damper example shows the capability of a Volterra-based model to release the source of differences between nonlinear and linear responses, specifically steady offset value, differences oscillation frequency, and phasing shift.

References

[1] Rugh, J. W., *Nonlinear System Theory*: *The Volterra/Wiener Approach*. John Hopkins University Press, 1981.

[2] Volterra, V., *Theory of Functionals and of Integral and Integro-Differential Equations*. Dover, New York, 1958.

[3] Prazenica, R., and Kurdila, A., "Multiwavelet Constructions and Volterra Kernel Identification," Nonlinear Dynamics Journal, Vol. 43, No. 3, 2006, pp. 277–310.

[4] Marzocca, P., Nichols, J., Milanese, A., Seaver, M., and Trickey, S., "Second-order spectra for quadratic nonlinear systems by Volterra functional series: Analytical description and numerical simulation," Mechanical Systems and Signal Processing Journal, Vol. 22, No. 8, 2008, pp. 1882-1895.

[5] Schurer, H., and Slump, H. and Herrmann, E.," Second order Volterra Inverses for Compensation of Loudspeaker Nonlinearity," IEEE ASSP Workshop on Applications of Signal Processing to Audio and Acoustics, 15-18 Oct. 1995, New York, USA .

[6] Kwon, J., Paik, I., and Chang, S., "Nonlinear Frequency Domain Analysis of Flexible Offshore Structures Using Volterra Series." KSCE Journal of Civil Engineering, Vol. 9, No. 5, 2005, pp. 391-401.

[7] Marzocca, P., Librescu, L., and Silva, W., "Aeroelastic Response of Nonlinear Wing Sections Using a Functional Series Technique," AIAA Journal, Vol. 40, No. 5, 2002, pp. 813–824.

[8] Marzocca, P., Silva, W., and Librescu, L., "Nonlinear Open-/Closed-Loop Aeroelastic Analysis of Airfoils via Volterra Series," AIAA Journal, Vol. 42, No. 4, 2004, pp. 673– 686.

[9] Wouw, N., Nijmwijer, H., and Campen , D., "A Volterra Series Approach to the Approximation of Stochastic Nonlinear Dynamics," Nonlinear Dynamics Journal, Vol. 27, No. 4, 2002, pp. 397-409.

[10] Omran, A., and Newman, B., "Nonlinear Analytical Multi-Dimensional Convolution Solution of the Second Order System," Journal of Nonlinear Dynamics, to Appear-DOI: 10.1007/s11071-010-9764-9.

[11] Omran A. and Newman B., "Nonlinear Cause-Effect Analysis for a Second Order System using Volterra Kernels,"ACC2010, IEEE American Control Conference, Baltimore, Maryland, June 30 - July 2,2010.

[12] Omran A. and Newman B., "Analytical Response for the Prototypic Nonlinear Mass-Spring-Damper System," ESDA2010 Proceedings of the ASME 10th Biennial Conference on Engineering System Design and Analysis, Istanbul, Turkey, July 12-14, 2010.

[13] Omran A. and Newman B., "Analytical Nonlinear Analysis Methodology for Reduced Aircraft Dynamical Systems," ICAS2010 Annual International Council of the Aeronautical Sciences Conference, Nice, France, September 19-24, 2010.

[14] Omran A. and Newman B., "Aircraft Volterra Parameter-Varying Modeling Approach," AIAA Atmospheric Flight Mechanics Conference and Exhibit, Toronto, Ontario, Canada, August 2-5, 2010.

[15] Omran, A. and Newman, B., "Piecewise Global Volterra Nonlinear Modeling and Characterization for Aircraft Dynamics," Journal of Guidance, Control, and Dynamics, Vol. 32, No. 3, May-June 2009, pp. 749-759.

[16] Omran A., and Newman B., "Global Aircraft Dynamics Using Piecewise Volterra Kernels," AIAA Atmospheric Flight Mechanics Conference and Exhibit, Honolulu, HI, USA, August 18-21., 2008.